Composites Science and Technology 69 (2009) 2649–2656

Contents lists available at ScienceDirect

Composites Science and Technology

journal homepage: www.elsevier.com/locate/compscitech

Multifunctional properties of high volume fraction aligned carbon nanotube polymer composites with controlled morphology

Hülya Cebeci [a,b], Roberto Guzman de Villoria [a], A. John Hart [c], Brian L. Wardle [a,*]

[a] Department of Aeronautics and Astronautics, Massachusetts Institute of Technology, Cambridge, MA 02139, USA
[b] Department of Aeronautical Engineering, Istanbul Technical University, Maslak, Istanbul 34469, Turkey
[c] Department of Mechanical Engineering, University of Michigan, Ann Arbor, MI 48108, USA

ARTICLE INFO

Article history:
Received 9 June 2009
Received in revised form 4 August 2009
Accepted 12 August 2009
Available online 19 August 2009

Keywords:
A. Carbon nanotubes
A. Polymer
A. Nano composites
B. Mechanical properties
B. Electrical properties

ABSTRACT

Advanced composites, such as those used in aerospace applications, employ a high volume fraction of aligned stiff fibers embedded in high-performance polymers. Unlike advanced composites, polymer nanocomposites (PNCs) employ low volume fraction filler-like concepts with randomly-oriented and poorly controlled morphologies due to difficult issues such as dispersion and alignment of the nanostructures. Here, novel fabrication techniques yield controlled-morphology aligned carbon nanotube (CNT) composites with measured non-isotropic properties and trends consistent with standard composites theories. Modulus and electrical conductivity are maximal along the CNT axis, and are the highest reported in the literature due to the continuous aligned-CNTs and use of an unmodified aerospace-grade structural epoxy. Rule-of-mixtures predictions are brought into agreement with the measured moduli when CNT waviness is incorporated. Waviness yields a large (~10×) reduction in modulus, and therefore control of CNT collimation is seen as the primary limiting factor in CNT reinforcement of composites for stiffness. Anisotropic electron transport (conductivity and current-carrying capacity) follows expected trends, with enhanced conductivity and Joule heating observed at high current densities.

1. Introduction

Bulk nanostructured composites combining existing advanced fibers, structural polymers, and carbon nanotubes (CNTs) with tailorable and enhanced macroscopic engineering properties are being developed by many groups for aerospace and other applications [1]. Development of such materials requires scaling and establishing long-range order of the nanostructures, and also an understanding of the properties of the constituents and how they interact [2–7]. Here, an aligned-CNT polymer nanocomposite (A-PNC) is fabricated using a high-performance (aerospace-grade structural epoxy) thermoset, and anisotropic multifunctional properties quantified and discussed relative to morphology of the samples. High volume fraction (V_f) continuous-CNT A-PNCs are fabricated via a novel mechanical densification [8] technique (see Fig. 1). This avoids the issue of dispersion, random orientation, and discontinuity (non-continuous CNTs) of the CNTs inherent in the extant work on PNCs which has focused almost solely on filler-like concepts [9–11]. Controlling morphology of the PNCs is critical for interpreting the multifunctional property results, and both SEM and X-ray scattering provide detailed quantification of PNC morphology herein. Randomly-oriented PNCs (R-PNCs) are also fabricated for comparison of unaligned vs. aligned reinforcement. Modulus and electrical conductivity are maximal along the CNT axis in A-PNCs, and are the highest reported to date due to the aligned CNT morphology and use of an unmodified aerospace-grade structural polymer [12,13], *e.g.*, the modulus is 1000× greater than recently reported for an elastomeric A-PNC [14], and the highest bulk conductivity (23 S/m) is reported for an epoxy PNC along the axis of the continuous CNTs. The measured modulus is in agreement with micromechanics predictions that consider waviness of the CNTs, and both modulus and electrical conductivity trends are consistent with standard physical models. Control of nanostructure morphology is essential for understanding and predicting properties of a broad array of new materials, including CNT-based fibers, 3D nano-engineered composites, and metamaterials [15–19].

Theoretical calculations and experimental measurements on individual CNTs show that these one dimensional materials have elastic moduli between 0.5 and 1 TPa and tensile strengths of perhaps 50–200 GPa [20–22] making them ideal reinforcement candidates for composites, and even more attractive given their low densities. From the existing literature, extensive efforts have focused on dispersing single or multiwalled CNTs in low modulus polymers for reinforcing thermoplastics [13,23] for applications such as electrically conducting composites [24].

* Corresponding author. Tel.: +1 617 252 1539; fax: +1 617 253 0361.
E-mail address: wardle@mit.edu (B.L. Wardle).

0266-3538/$ - see front matter © 2009 Elsevier Ltd. All rights reserved.
doi:10.1016/j.compscitech.2009.08.006

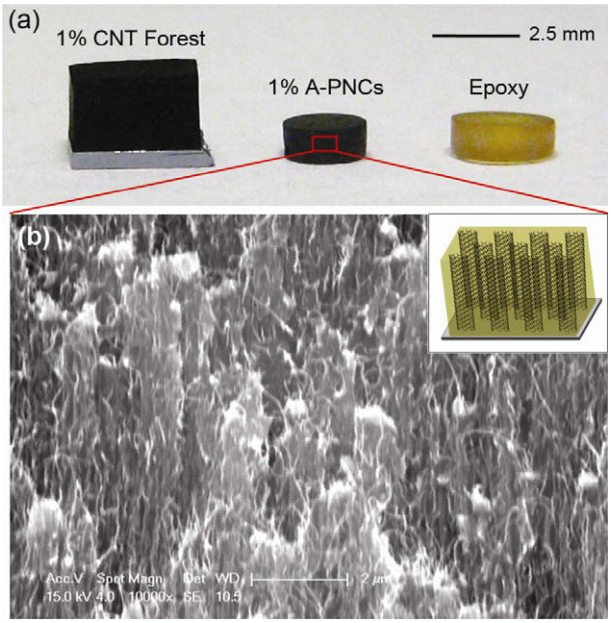

Fig. 1. Controlled-morphology polymer nanocomposites: (a) Image of 1% aligned-CNT forest, 1% A-PNCs and pure epoxy samples, (b) SEM image of 1% A-PNC fracture surface with an inset schematic of the CNT alignment direction. Scalebar is 2 μm.

However, the poor properties of these polymers and the necessary processing conditions make these nanocomposites unsuitable for advanced structural composites. Dispersion and distribution challenges limit the reinforcement volume fraction typically to below 5% of randomly-oriented CNTs. Alternatively, some researchers have focused on synthesizing aligned CNTs [25–28] and the combination of aligned and continuous CNTs with structural resins like epoxy could achieve maximal mechanical reinforcement and transport properties. In this work, both aligned and random PNCs are compared up to CNT volume fractions of 20% (A-PNCs only), close to practical and theoretical packing limits for 8–10 nm diameter CNTs.

2. Experimental

Fabrication of aligned-CNT and randomly-oriented CNTs polymer nanocomposites (A-PNCs and R-PNCs, respectively) are described before morphology characterization, mechanical, and electrical testing are discussed.

2.1. Polymer nanocomposite fabrication

First, continuous and aligned CNTs are grown for fabricating the A-PNC and R-PNC samples. MWNTs were grown using the thermal chemical vapor deposition (CVD) method on silicon wafers with a thin catalyst layers of Fe(catalyst)/Al_2O_3 (diffusion barrier)(1/10 nm) deposited by electron beam evaporation. CNT growth was performed in a (22 mm ID) quartz tube furnace (G. Finkenbeiner, Inc.) at atmospheric pressure using reactant gases of C_2H_4, H_2 and He (Airgas,75/400/125 sccm) [25]. Typical growth temperature was 750 °C, and average CNT growth rate was 2 μm s^{-1}. CNT forests were grown on 1 × 1 cm silicon wafers with coverage of well aligned 10^9–10^{10} CNTs. Growth time was 10 min with a typical forest height (continuous CNT length) of 1 mm.

The as-grown (1% volume fraction) CNT forests were released from the growth substrate and the free standing forests were compressed using a mechanical biaxial densification instrument to desired volume fractions (1%, 8%, and 20% V_f) [8]. The compressed forests (surfaces unmodified, unfunctionalized) were then transferred to a z-stage and lowered into an uncured epoxy pool just touching the top surface of epoxy. An aerospace-grade epoxy, RTM 6 (Hexcel), having viscosity of approximately 80 cP at 90 °C was used for this study. Infiltration of polymer into CNT forest was driven by capillary action which is strongly affected by inter-CNT spacing (volume fraction effect) and polymer viscosity. CNTs preserve their alignment during polymer infiltration to forest, and the epoxy is cured following the recommended procedure from the manufacturer as 1 hour at 160 °C and 2 hours at 180 °C, yielding the desired nanocomposites. The cured samples were machined and mechanically polished to achieve a smooth surface for characterization. As a result of the polishing and base-growth CNT processes, no Fe catalyst is present in the specimens. Thermogravimetric analysis (TGA) indicates the forests contain less than 10% amorphous carbon, which is deposited on the CNT sidewalls from the hydrocarbon atmosphere during growth [29]. Volume fractions for all samples are assessed by volumetric calculations. The A-PNC samples were fabricated at ~1%, 8%, and 20% volume fractions.

R-PNCs are fabricated by mixing a CNT forest with the epoxy resin. The mixture was placed between two Teflon plates that were sheared by hand for 10 min. After 10 min, the CNT/resin dispersion appeared homogeneous visually and was poured into a silicone mold with a spatula. The samples were cured and machined following the procedure indicated above for A-PNCs. Samples were fabricated for ~0.5%, 1%, 2%, and 4% volume fractions; 4% was the maximum volume fraction achieved due to processing difficulties arising from viscosity increase due to the CNTs.

2.2. Morphology characterization

The aligned and random CNT PNC morphologies were evaluated using scanning-electron microscopy (SEM), utilizing a JEOL 5910 and also a Philips XL 30, having resolutions of 1 μm and 50 nm, respectively. X-ray scattering studies allow CNT alignment within the polymer and polymer morphology to be assessed. X-ray scans were performed at the G1 beamline station at the Cornell High Energy Synchrotron Source (CHESS). The wavelength of the X-rays was 0.1239 nm, and the sample to detector distance was calibrated with silver behenate (first order scattering vector q of 1.076 nm^{-1}, with $q = 4\pi \sin(\theta/\lambda)$ where 2θ is the scattering angle and λ is the wavelength). Slit collimation was used to achieve a resulting beam spot that was approximately 0.2 mm in height and 0.4 mm in width (the y- and x-axes, respectively). A slow-scan CCD-based X-ray detector, home-built by Dr. M.W. Tate and Dr. S.M. Gruner of the Cornell University Physics Department, was used for data collection. Wide-angle X-ray scattering (WAXS) was performed using the same setup as SAXS but with a 40.5 mm sample-detector distance for capturing a wider scattering angle. WAXS therefore examines features on the sub-nanometer scale. The samples were placed on a motorized stage, which was moved relative to the fixed synchrotron beam and detector. For CNT forest and A-PNC samples, the samples were oriented with the direction of CNT alignment perpendicular to the X-ray beam, and along the vertical axis of the detector. The detector plane is perpendicular to the X-ray beam. The X-ray images shown later have the coordinate system and orientation of the detector.

2.3. Nanoindentation testing

Both A-PNCs and R-PNCs were tested via standard nanoindentation methods for modulus extraction. To achieve consistent results, the surfaces were mechanically polished in three steps with particle roughness ranging from 5 μm down to 0.005 μm. Surfaces were inspected under optical microscope before testing. The tests were performed using a Nanotest 600 nanomechanical testing system

(Micro Materials, UK). The nanoindenter monitors and records the load and displacement, which is capable of measuring and applying loads and depths ranging from 10 mN to 20 N (resolution ~100 nN) and up to 50 μm (resolution ~0.1 nm). Tests were performed inside the nanoindenter's thermally insulated environmental chamber (25 °C ± 0.5 °C) and relative humidity (45% ± 2%) with a Berkovich-type indenter. In order to compare the results obtained for the unreinforced epoxy matrix and the nanocomposites, the test's parameters were held constant, including importantly for polymers loading and unloading rates (100 mN/s respectively). Depending on the sample sizes, 12–16 indents were applied over the surface of each sample with a spacing of 350 μm. The samples were mounted on an aluminium stub and indented to 30 μm. Surface quality of the indents was ensured by SEM inspection after testing and results were averaged. Good surface quality via the three step polishing method yields highly repeatable (overlapping indentation curves) results. The load–displacement curves were analyzed to determine modulus using the Oliver–Pharr theory [30] where the unloading curve is used to obtain the reduced modulus (E_r). The reduced modulus is related to the specimen modulus through Eq. (1) for isotropic materials:

$$\frac{1}{E_r} = \frac{1-\nu^2}{E} + \frac{1-\nu_i^2}{E_i} \tag{1}$$

where E is the modulus of the sample, ν is the Poisson's ratio normal to loading of the sample, E_i is the indenter modulus, and ν_i is the indenter Poisson's ratio. The indenter is diamond with E_i = 1141 GPa and ν_i = 0.07, ν is assumed as 0.3 due to the matrix (polymer) dominated response in this direction, and because this yields the most conservative (lowest) calculation of modulus. Due to the aligned nature of the CNTs in most of the samples tested, the material is not isotropic and therefore when using the Oliver–Pharr theory and Eq. (1), the extracted modulus is referred to here as an effective modulus [31].

2.4. Electrical testing

A-PNC and R-PNC samples were measured for DC electrical resistivity in a double 2-probe configuration (see Fig. 5a). For A-PNCs, the bulk volume conductivity was measured in two directions, axial and transverse. Different sample sets for various volume fractions were used for transverse and axial directions. In the case of R-PNCs and the axial direction of A-PNCs, samples were small cylinders of 3–4 mm diameter by 1 mm length. For the transverse direction, the samples were 2 mm wide × 2 mm high × 1 mm long. Two opposite surfaces were used as contacts having silver-paint electrodes applied after being polished. One of these contacts was attached to a polished copper plate with silver paste. To measure the conductivity, the sample was placed on an automated stage, where the three axes were controlled. One metal probe was placed on the copper plate and the other on the bottom surface using the micro stage. A power supply (model HY 3005) and a voltammeter (HP 34401) were connected in parallel to the probes, in order to record the applied intensity and the difference of potential between the electrodes of the sample. The PNC surface temperature was measured with a thermal camera (PCE Group-TC3) supported by a tripod. The resistivity was calculated from the slope of the I–V curve normalized by the dimensions of the samples for intensities lower than ~0.5 A/cm^2, so that the sample temperature was always less than 75 °C. At least two different samples were measured for each reported conductivity value, with multiple measurements per sample performed. For consistency of measurements, the current was monitored until the temperature stabilized, and measurement was taken at least one minute after this stabilization.

3. Results and discussion

Polymer nanocomposites were fabricated from vertically-aligned multi-walled CNT forests (sometimes called VANTA, vertically-aligned nanotube arrays) grown via a modified chemical vapor deposition (CVD) process [25]. The resulting forests have been characterized previously for alignment, distribution and spacing [32]. A-PNCs were fabricated for various volume fractions via mechanical densification of the VANTA followed by capillary-induced wetting with an aerospace-grade thermoset epoxy (see Methods and Supporting Information). No functionalization of the CNT surfaces is made, the CNTs are used as-grown. Rather than

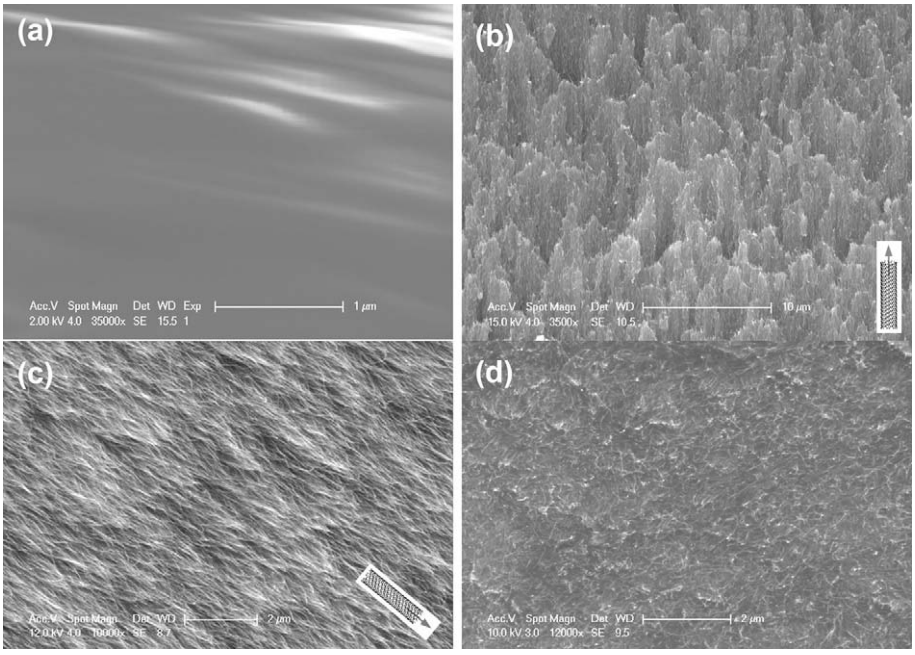

Fig. 2. SEMs of (a) Epoxy sample, (b) 1% Aligned-PNC, (c) 20% Aligned-PNC, (d) 4% Random-PNC. In images (b) and (c), the direction of CNT alignment is indicated. Scalebars are 1 μm, 10 μm, 2 μm, and 2 μm, respectively.

controlling volume fraction by mixing in greater quantities of filler (CNTs), volume fraction is varied by mechanical densification (reducing the inter-CNT spacing) in the same way that volume fraction is varied in aligned continuous fibers in advanced composites. Densification of aligned-CNT forests has also been achieved by other methods, *e.g.,* solvent evaporation [33], a process that lacks control of volume fraction and yields cells or voids in large-area forests that are unsuitable for creating uniform composites. In capillarity-driven wetting, polymers are pulled into a VANTA along the aligned CNT axis through capillary forces that develop between the CNTs. The same capillary mechanism has been used to fabricate advanced woven fiber composites containing aligned CNTs [34,35]. Randomly-oriented CNT PNCs (R-PNCs) are prepared using shear mixing allowing a maximum of only 4% volume fraction of CNTs.

3.1. Polymer nanocomposite morphology characterization

After preparing the variable volume fraction A-PNCs, their morphology is characterized by optical and scanning-electron microscopy (OM and SEM) and small and wide-angle X-ray scattering (SAXS and WAXS). R-PNC and A-PNC fracture surfaces (prepared cryogenically) for different volume fractions are shown in Fig. 2. The neat aerospace-grade resin (Hexcel RTM6) shows a relatively smooth surface (see Fig. 2a) whereas samples with A-CNTs have a surface morphology indicating both CNT alignment and packing as compared to R-PNCs. Increasing the volume fraction of the aligned CNTs from 1% to 20% alters the fracture surface significantly and also serves as a visual indication of alignment and effective wetting (Fig. 2b, c). The R-PNCs form a so-called good dispersion with a typical filler-like morphology as can be seen for 4% volume fraction of CNTs in Fig. 2d.

PNC morphology was investigated non-destructively by synchrotron X-ray scattering (see Methods Section). As shown in (Fig. 3a–b), neat epoxy exhibits a smoothly decaying scattering pattern with no significant features, whereas CNT addition causes a shoulder with position corresponding to the average diameter of CNTs in the X-ray beam path. For X-ray interpretation, the CNTs were modeled as hollow cylinders with a lognormal diameter distribution [36] to give D_{CNT} = 10.5 nm for all PNC samples, which is in close agreement with previous TEM measurements of 8–10 nm.

CNT alignment within the PNCs was quantified using the Hermans' orientation parameter (H) [37], calculated by azimuthal integration over a single quadrant of the scattering pattern, at the location of the CNT shoulder peak. A value of H = 1.0 indicates perfect vertical CNT orientation, H = 0 represents random orientation, and H = −0.5 represents perfect horizontal orientation [36]. As indicated by the scattering images and summarized in the Table 1, the H values are effectively zero for the randomly mixed R-PNCs and up to 0.5 for A-PNCs, with the highest in 20% V_f A-PNCs. The value of 0.5 is typical for an as-grown CNT forest before polymer infiltration, demonstrating that A-PNC fabrication in this work preserves the advantageous aligned morphology of the CNT forest.

Table 1
Summary of non-destructive SAXS measurements of CNT alignment within A-PNCs and R-PNCs.

Sample	CNT V_f %	Hermans' (H)
A-PNCs	1	0.37
	8	0.36
	20	0.46
R-PNCs	1	0.05
	2	0.01
	4	0.01

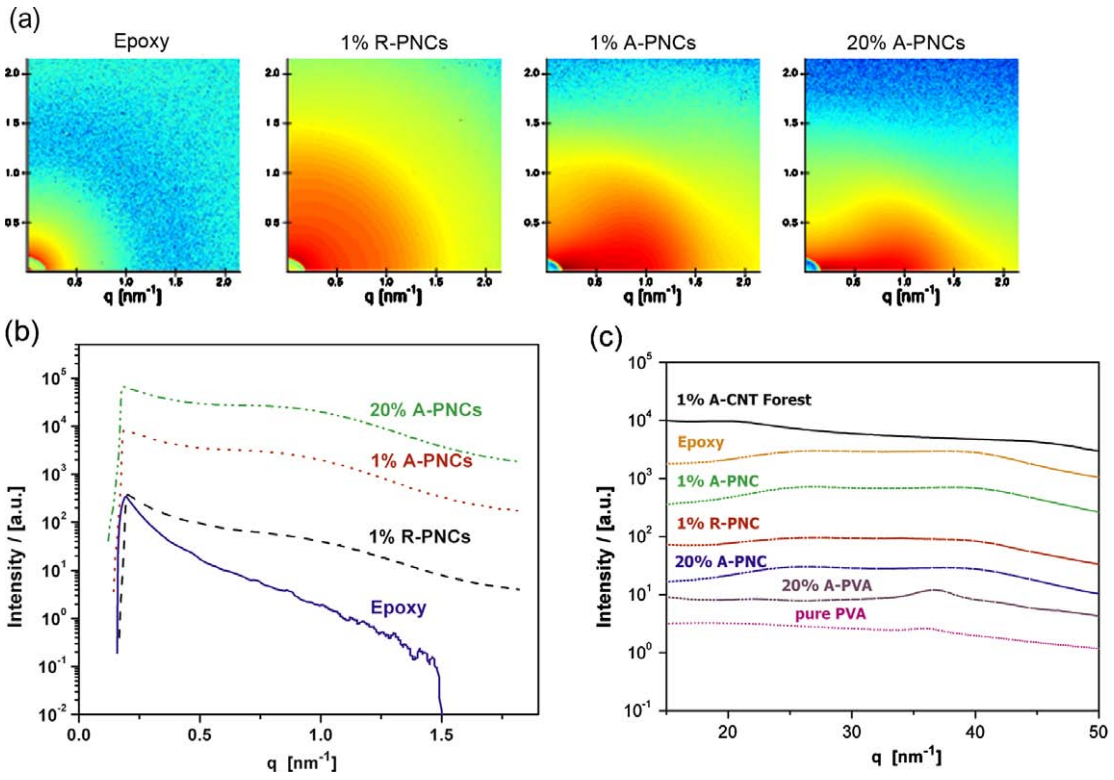

Fig. 3. (a) SAXS patterns of epoxy, A-PNCs and R-PNCs where asymmetric scattering indicates increasing alignment of CNTs within the matrix. (b) Integrated intensity curves from SAXS patterns of pure epoxy, A-PNCs and R-PNCs, showing a characteristic peak for monodisperse CNTs. The peak is more prominent at higher CNT V_f%'s. (c) WAXS analysis showing epoxy, A-PNCs, R-PNCs, pure PVA, A-PVA PNC, and A-CNTs.

CNTs have been shown to alter polymer packing and crystallinity [5], particularly for thermoplastics. Such interactions during the processing can confuse interpretation of PNC properties because the polymer phase has been altered by the formation of an interphase region which is estimated to be 10–100 nm in extent local to the CNT [6]. If such interphase estimates are correct, up to 100% of the polymer phase can be interphase in the PNCs studied here. While thermosets are less susceptible to creating an interphase, this possibility is directly assessed using WAXS because altered polymer properties are a critical feature in interpreting modulus results subsequently. The features in Fig. 3c are interpreted to be a simple superposition of the CNT and epoxy features, indicating that the epoxy has not formed a measurable interphase. By contrast, PVA was analyzed in the same way and a new peak is observed (Fig. 3c) at $q = 37\ nm^{-1}$, indicative of a change in polymer structure due to the presence of CNTs. Due to the WAXS information, the following discussion of PNC properties focuses on a simple 2-phase composite of CNTs and *unmodified* epoxy.

3.2. Modulus results and modeling

Despite the high measured modulus values reported for CNTs [38,39], PNCs have not demonstrated expected levels of stiffness improvement due to several key issues largely related to processing and morphology, *e.g.,* [40,41]. Mixing methods produce low volume fraction PNCs in a randomly-oriented configuration, and adhesion between the CNTs and the polymer is coupled to processing through functionalizations that is used to disperse and avoid agglomerations. Here, as-grown (unfunctionalized) forests are combined with unmodified (no solvents) epoxy to avoid this processing-property coupling. Since the modulus of a composite is a function of the fiber and matrix properties and their interaction, it is of interest to determine the reinforcing effect by comparing A-PNCs and R-PNCs at different volume fractions as in a typical fibrous composite characterization. Care must be taken when discussing the modulus of a hollow MWNT [42], and the approach taken here follows the current practice of using an effective modulus based on the total MWNT cross-sectional area [22], conservatively calculating the PNC modulus. The mechanical tests of nanocomposites were performed using standard nanoindentation loading–unloading curves and the effective elastic modulus (E) of the samples is obtained, using assumptions that give the most conservative calculation (see details in the Experimental section).

A linear trend in modulus is observed in Fig. 4 with increasing volume fraction of A-PNCs from the baseline epoxy, a trend consistent with standard composite mechanics predictions such as simple rule of mixtures or Mori–Tanaka. Modulus values of A-PNCs in Fig. 4a are the highest reported for epoxy resin, due to the CNT alignment at all volume fractions (for comparison with literature all the volume fraction values are converted to weight fractions in Fig. 4a [13]). The literature values in Fig. 4a are the highest reported at different weight fractions. Further, at high volume fraction, the modulus trend continues linearly, whereas in the extant data (Fig. 4a) the modulus increase falls off at high volume fractions which is usually attributed to poor dispersion. The A-PNC modulus is far from that expected given a simple rule of mixtures analysis considering collimated CNTs in a compliant matrix, *e.g.,* at 20% volume fraction aligned CNTs with a MWNT modulus of 0.5 TPa, the composite modulus is expected to be ~100 GPa, rather than 8.8 GPa measured here. Numerous morphological features play a role in determining the effective PNC physical properties, including degree of polymer bonding with the CNT, changes induced in the polymer packing and conformality (and possibly crystallinity), CNT functionalization and adsorbed surface species, microscopic voids in the polymer due to fabrication, CNT aspect ratio, distribution, agglomeration (bundling), and alignment, among others. It has already been demonstrated above that for the PNCs fabricated here the (thermoset) polymer morphology is not affected by the nanostructures (as expected for an epoxy), voids are not present in the well-consolidated samples, and CNT alignment is preserved in the PNC from the as-grown forest. We next examine the hypothesized dominant morphological feature on direction-dependent properties of the PNCs: CNT waviness effect on modulus, and continuity of the CNTs (unbroken, continuous) across the PNC sample on electrical conductivity.

CNT waviness has been modeled in PNCs by other authors [43–45] and is predicted to have a significant effect on both the axial (CNT axis) [44] and transverse PNC modulus [45]. Following the derivations in that prior work [44], the simple composite rule of mixtures model is modified by calculating a wavy CNT modulus, assuming the CNT has a sinusoidal form, as a function of the amplitude–wavelength ratio (a/λ) of the wavy CNT and the relative stiffness of the CNT vs. the matrix. The wavelength ratio is calculated from 75 high-resolution SEM measurements of CNT forests yielding a measured $a/\lambda = 0.185 \pm 0.10$. Using the analysis results from [44] with a E_{CNT}/E_m ratio of 100 (0.5 TPa MWNT axial modulus), an expected modulus at 20% V_f of 9–10 GPa is calculated which is in good agreement with our measured 8.8 GPa (see Fig. 4b). Furthermore, the linear tend of modulus with V_f observed experimentally is also predicted using this model. Waviness is therefore seen as the dominant feature affecting the A-PNC modulus, explaining the majority of the difference (10×)

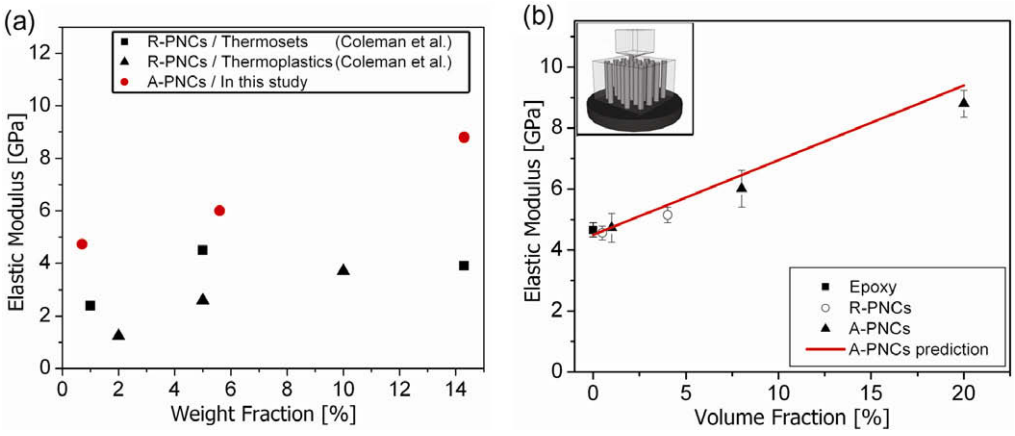

Fig. 4. (a) Comparison of A-PNC results to extant elastic modulus data [13]; (b) Elastic modulus effect investigation for aligned and random PNCs for various volume fractions. Inset: schematic representation of standard nanoindentation procedure by Berkovich indenter on A-PNC surface.

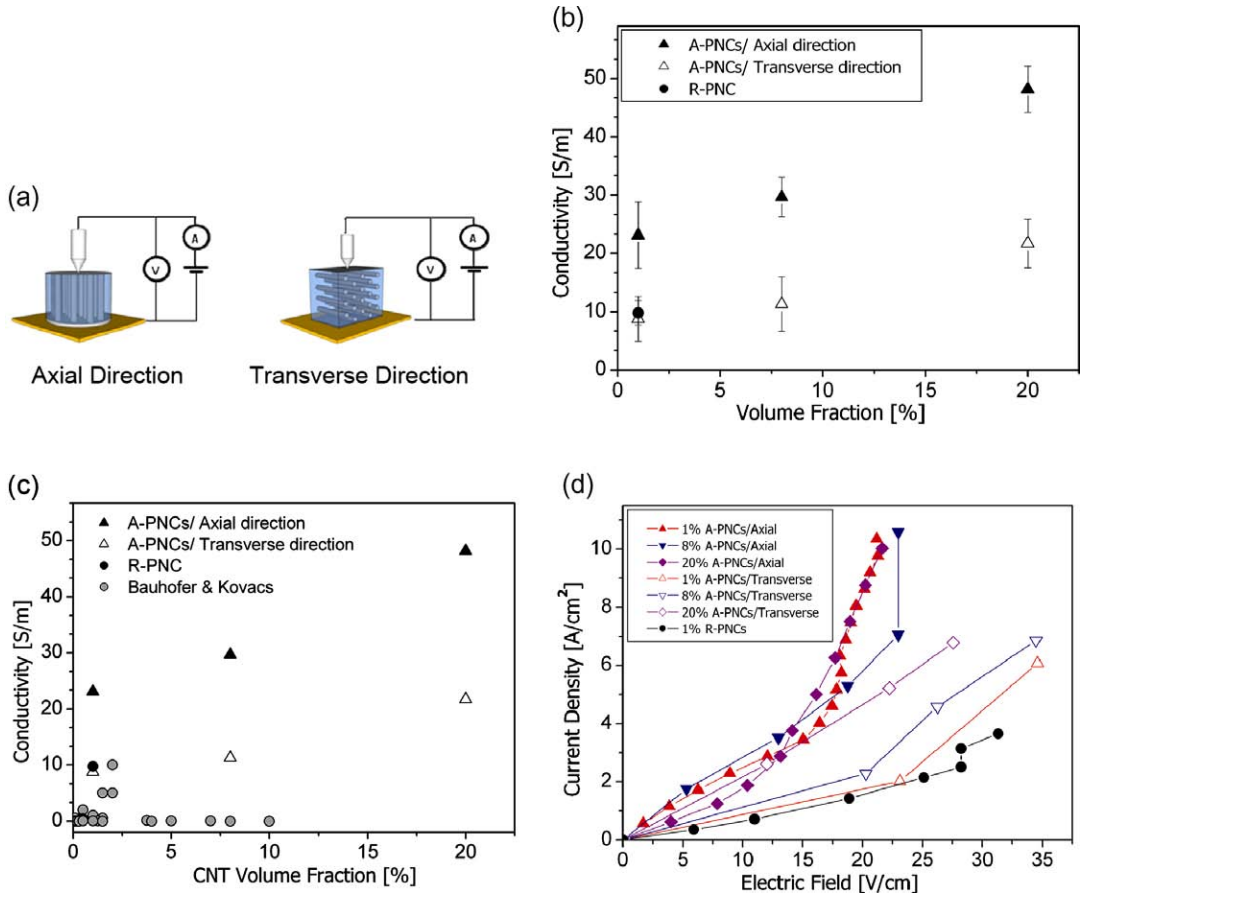

Fig. 5. (a) Schematic representation of A-PNCs for electrical resistivity measurements. (b) Electrical conductivity in the axial and transverse directions of the aligned and random PNCs. (c) Electrical conductivity of PNCs for different CNT volume fractions. Experimental data comparison from our work vs. recently summarized results [12]. (d) Field and current density variation exhibiting non-linearity due to Joule heating at higher current densities.

between the measured and the expected moduli, and is seen as the critical limiting factor for CNT reinforcement in PNCs. Bending and other effects, such as the bond between the CNT and the epoxy, must be considered small relative to the CNT waviness effect. The magnitude of the amplitude–wavelength ratio has a strong effect on the PNC modulus, *e.g.,* at a ratio of 0.02, the expected modulus would increase from 10 to 24–44 GPa (for 0.5–1 TPa CNT axial modulus at 20% V_f) giving a specific stiffness of 24–44 GPa cm^3/g, which is comparable (~35 GPa cm^3/g) to carbon aligned-fiber polymer composites [46] at the same volume fraction of reinforcement. Unaccounted for in the wavy nanotube models are effects associated with bending the CNTs (CNTs are treated as solids, not shells), which can be important in mechanical properties of PNCs [47].

3.3. Anisotropic electrical properties

The addition of conductive particles to an insulating polymer can result in an electrically conductive composite if the particle concentration exceeds the percolation threshold, defined as the particle volume fraction required to form a conductive network through the bulk polymer. CNTs are very effective fillers, with an electric current-carrying capacity cited to be as large as 1000 times higher than copper wires [48]. Electrical conductivity in PNCs usually focuses on a discussion of percolation threshold, either statistical, kinetic, or effective (considering tunneling) [12] using randomly-oriented CNTs with poorly quantified morphology. Many polymers have been investigated for percolation threshold and conductivity with randomly-oriented CNTs and the results reviewed by several authors [12,23,49]. There are clearly differences in electrical conductivity due to CNT features, especially distribution, degree of alignment, CNT–CNT and CNT–polymer interactions and hopping or tunneling behavior [50–52], but also differences due to the polymer and test methods (particularly surface resistivity testing of films vs. bulk resistivity measurements [53]). Here, at 1% CNT volume fraction, it is expected that conductivity in all directions is beyond the percolation threshold. Particularly noteworthy is that along the PNC axis, no percolation threshold is expected due to the continuous aligned-CNTs.

Direction-dependent volume (not surface converted to bulk) resistance has been measured in the axial and transverse directions as shown in Fig. 5a and used to calculate volume conductivity via the current density and electric field relationship $J = \sigma E$. In the axial direction, continuous CNTs span the sample leading to higher conductivity than in the transverse direction, *e.g.,* for the 1% V_f A-PNC, conductivity is 23 and 8.2 S/m for the axial and transverse directions, respectively (see Fig. 5b). In the transverse direction, CNT waviness and entanglement create a conductive path similar to percolation through the insulating epoxy. The measured axial conductivity is higher than all other reported epoxy PNC conductivities for a bulk PNC (see comparison to extant data from recent review paper [12] in Fig. 5c). Adding more CNTs per volume (*i.e.,* increasing the aligned CNT volume fraction as in a typical composite) increases the number of conductive paths which increases the conductivity linearly (see Fig. 5b). Consistent with the R-PNC morphology, 1% V_f R-PNC conductivity of 10 S/m is between the values for the A-PNC in the axial and transverse directions.

Finally, an important testing effect is identified in the extraction of electrical conductivity. Temperature rise (by thermal camera, see Experimental section) of the PNCs during the electrical measurements is monitored to verify the appropriate linear electrical conductivity. The conductivity has a significant non-linearity as the current density increases, with the non-linearity magnitude and onset varying depending on the PNC morphology (see Fig. 5d). Importantly, conductivity is *enhanced* due to the non-linearity making the range from which the resistance is extracted extremely important (the data in Fig. 5b is from the initial linear region of multiple samples). The non-linearity is attributed to Joule heating [54] measured via a thermal camera during testing, and also to some hysteretic effects (polymer degradation evidenced by smoke generation at high current densities in some tests). In the case of R-PNCs and transverse A-PNCs, the samples undergo thermal degradation (smoke is observed in some tests) after reaching temperatures higher than 160 °C. We hypothesize that the conductive aligned CNTs, acting like resistors in parallel, effectively carry all of the current density in the PNC sample, making the local temperature of the CNTs greater than 160 °C (the RTM6 epoxy maximum service temperature is quoted as 180 °C). The thermal camera integrates temperature over the sample, and nanoscale temperature variation (CNT to CNT for example) cannot be distinguished. Consistent with the higher PNC conductivity with volume fraction, current-carrying capacity is also enhanced as more conducting CNT channels are added (higher CNT volume fraction). For axial measurements of A-PNCs at 10 A/cm^2, the temperature of the samples are 91, 79, and 73 °C for 1%, 8%, 20% volume fraction, respectively, indicating higher current-carrying capacity as more aligned CNTs are introduced into the conducting network. The axial direction of the A-PNCs (continuous CNTs) carry more current than the transverse direction (and R-PNCs) as expected.

4. Conclusions and recommendations

The inclusion of aligned CNTs in bulk materials such as existing advanced composites is an important step forward in engineering materials, and can provide several advantages including tailoring and manufacturability of complex architectures. Control of nanoscale morphology in polymer nanocomposite as demonstrated herein allows measured properties to be appropriately interpreted. The results and trends in this study demonstrate anisotropic behavior via morphology control makes clear the classic structure–property linkage for PNCs that has been unclear to date in the literature. Further, appropriate morphology control and characterization allow dominant nanoscale interactions to be interpreted. CNT waviness is identified as a limiting factor on CNT reinforcement in composites, requiring very fine (micro to nanoscale control) of CNT waviness to reach significant modulus contributions from the CNTs. Such observations extend to other properties such as phonon transport in CNTs and PNCs where thermal boundary resistance, in addition to morphology, will contribute significantly to the effective PNC thermal properties. Results from this work support the feasibility of CNT use in structural composites for tailoring and enhancing multifunctional properties of bulk materials [16,34,55], and demonstrates the importance of controlling and characterizing nanostructure morphology in the same way that microstructure is controlled for existing advanced structural composites.

Acknowledgements

This study was supported by Airbus S.A.S., Boeing, Embraer, Lockheed Martin, Saab AB, Spirit AeroSystems, Textron Inc., Composite Systems Technology, and TohoTenax Inc. through MIT's Nano-Engineered Composite aerospace STructures (NECST) Consortium. Hülya Cebeci acknowledges support from Scientific and Technical Research Council of Turkey (TUBITAK) for a 2214-International Research Fellowship Programme. Roberto Guzman de Villoria is grateful for the support of the Ministry of Science and Education (MEC) for the award of a FPU grant (AP-2004-6264). The authors gratefully acknowledge Patrick Boisvert for SEM imaging, Peter Morley for specimen preparation assistance, Alan Schwartzmann for nanoindentation testing and Eric Verploegen and Jeremy Ng for SAXS/WAXS analysis. The authors are grateful for the donation of materials from Hexcel Corp.

References

[1] Dresselhaus MG, Dresselhaus G, Eklund PC. Science of fullerenes and carbon nanotubes. New York, (NY), San Diego, (CA): Academic Press; 1996.
[2] Wagner HD. Nanocomposites – paving the way to stronger materials. Nat Nanotechnol 2007;2:742–4.
[3] Njuguna B, Pielichowski K. Polymer nanocomposites for aerospace applications: properties. Adv Eng Mater 2003;5:769–78.
[4] Njuguna J, Pielichowski K. Polymer nanocomposites for aerospace applications: characterization. Adv Eng Mater 2004;6:204–10.
[5] Coleman JN, Cadek M, Ryan KP, et al. Reinforcement of polymers with carbon nanotubes. The role of an ordered polymer interfacial region. Experiment and modeling. Polymer 2006;47:8556–61.
[6] Winey KI, Vaia RA. Polymer nanocomposites. MRS Bull 2007;32:314–9.
[7] Suhr J, Koratkar N, Keblinski P, Ajayan P. Viscoelasticity in carbon nanotube composites. Nat Mater 2005;4:134–7.
[8] Wardle BL, Saito DS, Garcia EJ, et al. Fabrication, characterization of ultrahigh-volume-fraction aligned carbon nanotube–polymer composites. Adv Mater 2008;20:2707.
[9] Schulte K, Windle AH. Carbon nanotube (CNT) – polymer composites. Compos Sci Technol 2007;67:777. Special issue.
[10] Thostenson ET, Li CY, Chou TW. Nanocomposites in context. Compos Sci Technol 2005;65:491–516.
[11] Thostenson ET, Ren ZF, Chou TW. Advances in the science and technology of carbon nanotubes and their composites: a review. Compos Sci Technol 2001;61:1899–912.
[12] Bauhofer W, Kovacs JZ. A review and analysis of electrical percolation in carbon nanotube polymer composites. Compos Sci Technol 2009;69:1486–98.
[13] Coleman JN, Khan U, Blau WJ, Gun'ko YK. Small but strong: a review of the mechanical properties of carbon nanotube–polymer composites. Carbon 2006;44:1624–52.
[14] Ci L, Suhr J, Pushparaj V, Zhang X, Ajayan PM. Continuous carbon nanotube reinforced composites. Nano Lett 2008;8:2762–6.
[15] Li YL, Kinloch IA, Windle AH. Direct spinning of carbon nanotube fibers from chemical vapor deposition synthesis. Science 2004;304:276–8.
[16] Veedu VP, Cao AY, Li XS, et al. Multifunctional composites using reinforced laminae with carbon-nanotube forests. Nat Mater 2006;5:457–62.
[17] Gao JB, Yu AP, Itkis ME, et al. Large-scale fabrication of aligned single-walled carbon nanotube array and hierarchical single-walled carbon nanotube assembly. J Am Chem Soc 2004;126:16698–9.
[18] Zhang M, Fang SL, Zakhidov AA, et al. Strong, transparent, multifunctional, carbon nanotube sheets. Science 2005;309:1215–9.
[19] Allen SM, Thomas EL. The structure of materials. John Wiley & Sons; 1999.
[20] Treacy MMJ, Ebbesen TW, Gibson JM. Exceptionally high Young's modulus observed for individual carbon nanotubes. Nature 1996;381:678–80.
[21] Wong EW, Sheehan PE, Lieber CM. Nanobeam mechanics: elasticity, strength, and toughness of nanorods and nanotubes. Science 1997;277:1971–5.
[22] Yu MF, Lourie O, Dyer MJ, et al. Strength and breaking mechanism of multiwalled carbon nanotubes under tensile load. Science 2000;287:637–40.
[23] Moniruzzaman M, Winey KI. Polymer nanocomposites containing carbon nanotubes. Macromolecules 2006;39:5194–205.
[24] Eklund P, Ajayan P, Blackmon R, Hart AJ, Kong J, Pradhan B, et al. International assessment of carbon nanotube manufacturing and applications final report. WTEC, Inc.; 2007.
[25] Hart AJ, Slocum AH. Rapid growth and flow-mediated nucleation of millimeter-scale aligned carbon nanotube structures from a thin-film catalyst. J Phys Chem B 2006;110:8250–7.
[26] Hata K, Futaba DN, Mizuno K, et al. Water-assisted highly efficient synthesis of impurity-free single-waited carbon nanotubes. Science 2004;306:1362–4.
[27] Pan ZW, Xie SS, Chang BH, et al. Very long carbon nanotubes. Nature 1998;394:631–2.
[28] Fan SS, Chapline MG, Franklin NR, et al. Self-oriented regular arrays of carbon nanotubes and their field emission properties. Science 1999;283:512–4.
[29] Meshot EM, Tawfick S, Plata DL, Verploegen E, Hart AJ. Decoupled thermal treatment of precursor and catalyst enables engineering of diameter, structural quality, and growth kinetics of vertically aligned carbon nanotubes. ACS Nano 2009. doi:10.1021/nn900446a.
[30] Oliver WC, Pharr GM. Measurement of hardness and elastic modulus by instrumented indentation: advances in understanding and refinements to methodology. J Mater Res 2004;19:3–20.

[31] Qi HJ, Teo KBK, Lau KKS, et al. Determination of mechanical properties of carbon nanotubes and vertically aligned carbon nanotube forests using nanoindentation. J Mech Phys Solids 2003;51:2213–37.
[32] Hart AJ, Slocum AH. Force output, control of film structure, and microscale shape transfer by carbon nanotube growth under mechanical pressure. Nano Lett 2006;6:1254–60.
[33] Futaba DN, Hata K, Yamada T, et al. Shape-engineerable and highly densely packed single-walled carbon nanotubes and their application as super-capacitor electrodes. Nat Mater 2006;5:987–94.
[34] Garcia EJ, Wardle BL, Hart AJ, Yamamoto N. Fabrication and multifunctional properties of a hybrid laminate with aligned carbon nanotubes grown in situ. Compos Sci Technol 2008;68:2034–41.
[35] Garcia EJ, Hart AJ, Wardle BL, Slocum AH. Fabrication of composite microstructures by capillarity-driven wetting of aligned carbon nanotubes with polymers. Nanotechnology 2007;18.
[36] Wang BN, Bennett RD, Verploegen E, Hart AJ, Cohen RE. Quantitative characterization of the morphology of multiwall carbon nanotube films by small-angle X-ray scattering. J Phys Chem C 2007;111:5859–65.
[37] Alexander LE. X-ray diffraction methods in polymer science. New York: John Wiley & Sons; 1969 [National Institute of General Medical Sciences under award DMR-0225180].
[38] Poncharal P, Wang ZL, Ugarte D, de Heer WA. Electrostatic deflections and electromechanical resonances of carbon nanotubes. Science 1999;283:1513–6.
[39] Salvetat JP, Bonard JM, Thomson NH, Kulik AJ, Forro L, Benoit W. Mechanical properties of carbon nanotubes. Appl Phys A 1997;69:255–60.
[40] Thostenson ET, Chou TW. Aligned multi-walled carbon nanotube-reinforced composites: processing and mechanical characterization. J Phys D Appl Phys 2002;35:L77–80.
[41] Thostenson ET, Chou TW. On the elastic properties of carbon nanotube-based composites: modelling and characterization. J Phys D Appl Phys 2003;36:573–82.
[42] Pantano A, Boyce MC, Parks DM. Nonlinear structural mechanics based modeling of carbon nanotube deformation. Phys Rev Lett 2003;91.
[43] Bradshaw RD, Fisher FT, Brinson LC. Fiber waviness in nanotube-reinforced polymer composites-II: modeling via numerical approximation of the dilute strain concentration tensor. Compos Sci Technol 2003;63:1705–22.
[44] Fisher FT, Bradshaw RD, Brinson LC. Effects of nanotube waviness on the modulus of nanotube-reinforced polymers. Appl Phys Lett 2002;80:4647–9.
[45] Fisher FT, Bradshaw RD, Brinson LC. Fiber waviness in nanotube-reinforced polymer composites-1: modulus predictions using effective nanotube properties. Compos Sci Technol 2003;63:1689–703.
[46] Grimes GC. Composite materials: testing and design, vol. 10. ASTM International; 1992.
[47] Pantano A, Boyce MC, Parks DM. Mechanics of axial compression of single and multi wall carbon nanotubes. J Eng Mater Technol 2004;126:184–279.
[48] Collins GP. Different stripes – physicists struggle to explain high-temperature superconductivity. Sci Am 2000;283:33.
[49] Winey KI, Kashiwagi T, Mu MF. Improving electrical conductivity and thermal properties of polymers by the addition of carbon nanotubes as fillers. MRS Bull 2007;32:348–53.
[50] Park C, Wilkinson J, Banda S, et al. Aligned single-wall carbon nanotube polymer composites using an electric field. J Polym Sci Pol Phys 2006;44:1751–62.
[51] Li C, Thostenson ET, Chou TW. Effect of nanotube waviness on the electrical conductivity of carbon nanotube-based composites. Compos Sci Technol 2008;68:1445–52.
[52] Li CY, Thostenson ET, Chou TW. Dominant role of tunneling resistance in the electrical conductivity of carbon nanotube-based composites. Appl Phys Lett 2007;91.
[53] Valdes LB. Effect of electrode spacing on the equivalent base resistance of point-contact transistors. In: Proceedings of the IRE 1952. p. 1429–34.
[54] Kuroda MA, Leburton JP. Joule heating induced negative differential resistance in freestanding metallic carbon nanotubes. Appl Phys Lett 2006;89.
[55] Garcia EJ, Hart AJ, Wardle BL. Long carbon nanotubes grown on the surface of fibers for hybrid composites. AIAA J 2008;46:1405–12.